International Journal of Recent Development in Engineering and Technology
Website: www.ijrdet.com (ISSN 2347-6435(Online) Volume 14, Issue 12, December 2025)

Evaluating Thermal Insulation of Photo Thermal Roofs for Diverse Climatic Conditions: An Experimental and Numerical Approach.

Malik Burhan Ahmad[1], Er. Shilpa Chauhan[2]

[1]*M.Tech Student,* [2]*Asst. Professor, University School of Engineering & Technology, Rayat Bahra University, Mohali, India*

***Abstract*-- This research delves into the potential of solar architecture systems in bringing down building energy demand, contributing to the "Dual-carbon" initiative. The thermal performance of a solar-thermal roof in hot summer and cold winter zones, developing a model to assess its insulation capabilities, was explored. Exploratory and simulation outputs revealed that the solar-thermal roof surpasses standard or traditional roofs with regard to heat transmission and thermoregulation. Primarily, altering the gush in collectors can upgrade the solar-thermal roof's performance. Moreover, the roof's insulation properties are stoic by water saturation and insulation material thickness compared to standard or traditional roofs. These findings present valuable breakthrough for energy saving roof design in new buildings and reconstructed structures.**

***Keywords*-- Thermal Insulation, Energy Efficient, Photo Thermal Roof, and Energy Distribution.**

I. INTRODUCTION

The "Dual-carbon" plan, examines the peak carbon outpouring and netzero carbon emission, is a pivotal initiative for a green future. Lowering fossil fuel utilization and carbon emissions is necessary to accomplish the grail. With buildings accountable for a substantial amount of global energy demand and greenhouse gas emissions, it's vitally important to prioritize building energy conservation and sustainable energy technologies. By surveying building energy preservation plan, we can make noteworthy progress in the direction of meeting the "Dual-carbon" plan's aim.

Introduction to Photovoltaic/Thermal Systems: Aiming for eco-friendly building innovations, photovoltaic/thermal (PV/T) systems drew interest attributable to their inexhaustible and unpolluted nature. These setups, which incorporate photovoltaic panels and solar collectors, offer a viable approach for building energy conservation. Though various researchers have optimized the energy efficiency and economic feasibility of photovoltaic/ thermal systems, there is an increasing demand to understand their significance on building thermal characteristics.

Research Background: Evidence suggests that solar thermal collectors and photovoltaic panels desegragated with buildings can reach blazing temperatures, determining building energy consumption and indoor environmental comfort. The temperature of solar collectors used for domiciliary hot water is typically steady, but fluid temperature fluctuations can effect the indoor thermal conditions.

Research Objective: This paper aims to examine the thermal efficiency of a roof furnished with a field of thermal solar collectors with an air gap, compared to a traditional sloping roof in hot summer and cold winter conditions. The research examines the impact of water saturation of roof insulation covering on roof heat transfer and the insulation performance of the photo-thermal roof under different situations. The findings of this study provide a speculative basis for the application of photo-thermal roofs in building energy conservation.

II. METHODOLOGY

Experimental Setup: The experiment was supervised on the top floor of a residential building, located in Jammu at 74.86167°E longitude and 32.73528° N latitude. The experimental roof structure consisted of multiple layers to suit the region’s hot and cold climate. The experimental roof has a layered structure, consisting of:

40 mm reinforced concrete (top layer)

90 mm mineral wool board (insulation layer)

20 mm cement mortar

120 mm reinforced concrete (main structural layer)

20mm cement mortar (bottom layer).

Two experimental rooms were set up: one with a photo-thermal roof and the other with a conventional roof. The photo-thermal roof featured 10 solar collectors, each measuring 2000 mm × 1000 mm × 106 mm, covering an area of 5.6 m × 5 m. The water temperature was managed by acclimatizing the flow rate.

International Journal of Recent Development in Engineering and Technology
Website: www.ijrdet.com (ISSN 2347-6435(Online) Volume 14, Issue 12, December 2025)

Both of the rooms were aerated (cooling and heating) and monitored from 08:00 to 20:00 to assess the thermal performance.

Fig.1: Photovoltaic Panels

Data Collection: Temperature readings were taken using K-type thermocouples with high accuracy (Level 1) and minimal uncertainty (<0.1%). The experimental room equipped with air conditioning was monitored under summer conditions. Temperature detectors were purposively mounted on the roof surfaces, in an inactive area 1m down the ceiling and at the water inlet/ outlet. Key temperature determination included roof surface temperatures (both interior and exterior), water inflow and outflow temperatures, and ambient temperature. A PC- data acquisition system recorded real-time readings, while solar irradiance was measured by pyranometer type of radiation monitor (TBQ-2) at the designated location.

Theoritical Model:

Heat Transfer Analysis: For the photovoltaic roof solar radiation is partially reflected by the collector's glass cover, while the bulk is assimilated and converted into heat. This heat is then transmitted to the heat-carrying fluid which takes it away. Some heat elevates the collector's temperature, leading to heat dispersion into the environment through convection and radiation. A portion of this residual heat is transferred to the room through the roof.

International Journal of Recent Development in Engineering and Technology
Website: www.ijrdet.com (ISSN 2347-6435(Online) Volume 14, Issue 12, December 2025)

Conversely, the typical roof receives direct beam radiation, rising its temperature. This heat is then transferred directly through the roof.

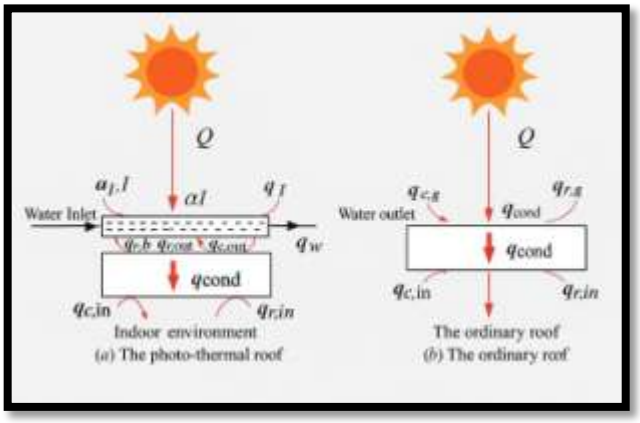

Fig.2*:* Roof Heat Transmission Model

Energy Balance Equation: The heat transfer model is determined by the energy balance equation, stated as:

$$\partial/\partial\tau\ (\rho E) + \nabla[\rightarrow u(\rho E + P)] = \nabla[k_e \nabla T - \sum j\ hj \rightarrow Jj + (\tau eff \rightarrow u)] + S_h$$

Where,

$\partial/\partial\tau\ (\rho E)$ = Rate of change of internal energy density (ρE) over time (τ). ρ is density and E is specific internal energy.

$\nabla[\rightarrow u(\rho E + P)]$ = Advective tranport of energy which represents the energy flux due to the fluid's velocity $\rightarrow u$ and pressure (P).

$\nabla[k_e \nabla T$ = Heat conduction due to thermal conductivity (k_e) and temperature gradient ∇T .

$-\sum j\ hj \rightarrow Jj$ = Energy transport due to diffusion of species.

$(\tau eff \rightarrow u)$ = Work done by viscous forces

S_h = Represents external heating and cooling mechanisms.

Given the small layer thinness of material in solar panels and roofs in proportion to their length and width, heat conduction can be approximated as unidirectional along the z-direction. By ignoring diffusion and viscosity dissipation, the equation reduces to:

$$\partial/\partial\tau\ (\rho E) + \nabla \rightarrow u\rho E = \nabla(k_e \nabla T) + S_h$$

Where,

$\partial/\partial\tau\ (\rho E)$: Represents the rate of change of total energy per unit volume within a control volume.

$\nabla \rightarrow u\rho E$: Represents the convective transport of total energy.

$\nabla(k_e\ \nabla T)$: Represents the heat conduction of thermal energy.

S_h: Represents the volumetric heat source within the system.

Collector Energy Balance: Concentrating on the collector as the research object, the energy balance equation may be written as:

$$\rho C\ \partial T/\partial\tau = (1 - \rho g)I - k_p\ \partial^2 T/\partial z^2 - S$$

This equation illustrates the energy balance for the collector, accounting for absorbed solar radiation, heat conduction, and other contributing elements.

The energy balance equations for the collector and roofs are fundamental to understanding the modes of heat transfer. For the collector, the energy balance equation accounts for energy accumulation, thermal gain, conduction of heat, and thermal loss. The thermal loss term comprises of radiation and convection to the environment, as well as thermal loss caused by fluid heating.

Heat Loss Term: The heat loss term (S_h) can be expressed as:

$$S_h = h_g(T_g - T_{o,a}) + \sigma\varepsilon_g(T_g^4 - T_{sky}^4) + \sigma\varepsilon_g\ (T_b^4 - T_{o,w}^4) / (1/\varepsilon_b + 1/\varepsilon_{o,w} - 1) + q_w$$

Photo-Thermal Roof Energy Balance: The energy balance equation for the photo-thermal roof is:

$$\rho C\ \partial t/\partial\tau = S_h - k_e\ \partial^2 T/\partial z^2 - h_i(T_{i,w} - T_i^a) - \sigma\varepsilon_{i,}^{\ w}(T_{i,w}^4 - T_n^4)$$

where,

$\rho C\ \partial t/\partial\tau$: Represents the rate of change of internal energy within the material.

S_h: Represents the heat gain of the photo-thermal roof, primarily due to radiant heat transfer between the collectors and the roof.

$-k_e\ \partial^2 T/\partial z^2$: Heat conduction within the material.

$-h_i(T_{i,w} - T_i^a)$: Convective heat tranfer between a surface at $T_{i,w}$ and a fluid at temperature T_i^a.

$-\sigma\varepsilon_{i,}^{\ w}(T_{i,w}^4 - T_n^4)$: Represents radiative heat transfer.

Ordinary Roof Energy Balance: Conversely, the normal roof's energy balance equation is:

$$\rho C\ \partial T/\partial\tau = S_h - k_e\ \partial^2 T/\partial z^2 - h_i\ (T_{i,w} - T_{i,a}) - \sigma\varepsilon_{i,}^{\ w}(T_{i,w}^4 - T_n^4)$$

International Journal of Recent Development in Engineering and Technology
Website: www.ijrdet.com (ISSN 2347-6435(Online) Volume 14, Issue 12, December 2025)

where,

$\rho C\, \partial T/\partial \tau$: The rate of energy storage in internal energy .

S_h: Represents the heat gain of the ordinary roof, primarily due to direct solar irradiation.

- $k_e\, \partial^2 T/\partial z^2$: Heat conduction

- $h_i\, (T_{i,w} - T_{i,a})$: Convective heat transfer between internal surface and the surrounding fluid.

- $\sigma \varepsilon_{i,}^{w}(T_{i,w}^{4} - T_n^{4})$: Radiative heat transfer between internal surface and its surroundings.

Effective Thermal Conductivity: The heat entering a room through a roof is guided by the effective thermal conductivity of the insulation material. When the heat on the roof's outer surface and the roof structure are constant, the heat transferred into the room is directly related to the effective thermal conductivity of the insulation material.

Porous Media: Insulation materials are usually perforated media filled with air and moisture. The volumetric ratio of air and water changes with atmospheric temperature and humidity. The material can be shown as a mixture of solid-phase insulation material, liquid-phase water and air, satisfying:

$$\varepsilon_s + \varepsilon_l + \varepsilon_a = 1$$

Water Saturation: The volume of liquid water can be expressed as water saturation:

$$\phi = \varepsilon_l / (\varepsilon_l + \varepsilon_a)$$

Effective Thermal Conductivity Models: The effective thermal conductivity of the insulation material can be calculated using different models.

For a parallel heat conduction model:

$$k_{ep} = k_s\varepsilon_s + k_l\varepsilon_l + k_a\varepsilon_a$$

For a series heat conduction model:

$$k_{ec} = 1 / (\varepsilon_s/k_s + \varepsilon_l/k_l + \varepsilon_a/k_a)$$

In fact, the effective thermal conductivity lies between these two extreme conditions:

$$k_{ec} \le k_e \le k_{ep}$$

Mineral Wool Board: In this research rock wool board with a porosity of 90% was used as the roof insulation material. The apparent thermal conductivity was determined using:

$$ke = (kep + kec) / 2$$

This simplification considers the intricate heat transfer mechanisms in the mineral wool board, inclusive of the inclined lapping of monofilament fibers and the random distribution of slag balls and liquid water.

Effective Thermal Conductivity vs. Water Saturation: The parallel thermal resistance model shows a linear rise in effective thermal conductivity with water saturation. However, the serial heat conduction model shows a modest rise in effective thermal conductivity up to 75% water saturation, followed by a sharp spike. The effective thermal conductivity calculated also increases with water saturation, with considerable fluctuation. A 0% to 100% increase in water saturation results in a 922.3% increase in effective thermal conductivity. Even a small increase in water saturation from 0% to 25% leads to a 53.7% increase in effective thermal conductivity.

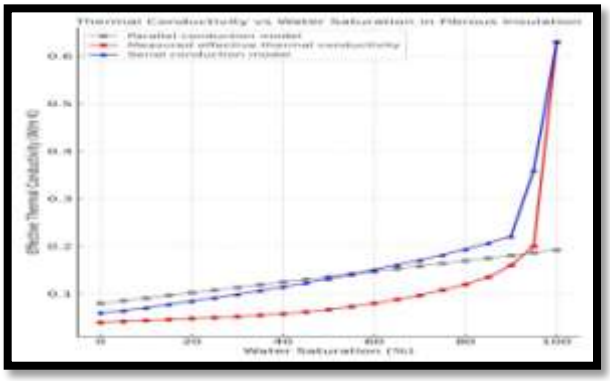

Fig. 3: Water Saturation effect on Insulation Performance.

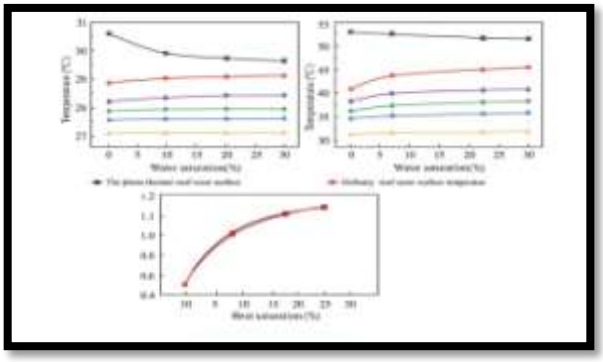

Fig. 4: Effect of water saturation on the heat flux of roofs.

Simulation Conditions: To compare the thermal performance of photo-thermal and conventional roofs, numerical simulations were performed using ANSYS FLUENT software.

International Journal of Recent Development in Engineering and Technology
Website: www.ijrdet.com (ISSN 2347-6435(Online) Volume 14, Issue 12, December 2025)

Two physical models were developed: a simplified 3D model of an air-conditioned room with a photo-thermal roof and an ordinary air-conditioned room with a conventional roof. To streamline the model, a single unit width of the collector's water pipe and surrounding components was analyzed.

Model Simplification: To reflect the limited cooling capacity of the air conditioner, the top floor room's air space was segemented into two zones: a non-occupied area (1000 mm below the roof) and a personnel occupied area. The air conditioner maintained a consistant temperature of 26 °C in the working area. To simplify the model, only 0.5 m of the indoor air-conditioned area and its upper space components were simulated, focusing on the non-working zone and the area 0.5 m below it.

Table 1:
Properties Of Layers Of Materials Used

S.NO.	Layers Of Materials	Dimensions *(a.b.c mm^3)*	Density *(kg/m^3)*	Massive Heat Capacity *(J/kg.K)*	Thermal Conductivity *(W/m.K)*
1	Absorber Plate	1000× 2000 × 1.5	2710	870	201.4
2	Copper Pipe	08× 2000 × 08	8988	380	386.3
3	Glass Cover	1000× 2000 × 4.5	2500	820	0.70
4	Air Layer In Collector	1000× 2000 × 4.5	1.500	1000	0.024
5	Air Layer	3000× 4000 × 100	1.500	1000	0.022
6	Insulation In Collector	1000× 2000 × 55	40	1350	0.04
7	Reinforced Concrete Layer	1000× 2000 × 150	2500	850	1.70
8	Cement Mortar Layer	1000× 2000 × 40	2000	830	0.82
9	Insulation Layer	1000× 2000 × δ	100	740	0.04

Numerical Model: The minimum dimensions of the numerical model were 134 mm × 2000 mm × (δ + 1906) mm.
Where,
δ represents the thickness of the roof's insulation layer.

The model featured a solar collector with water pipes (8 × 2000 × 8 mm) spaced 126 mm apart. The components in the model consisted of general materials with standard dimensions.

Simulation Parameters: The simulation employed a solar ray tracing model configured for a geographical location set to 32.73528° N, 74.86167° E, and a time zone of +8. Ideal weather conditions were assumed, with cloudless skies. The simulation time was adjusted to capture varying solar radiation conditions. The Discrete Ordinates (DO) radiation model was selected, with an enhanced angular discretization for more improved results. The k-ε turbulence model was used for its high accuracy.

Table 2:
Meteorological Parameters During Summer In Jammu City

S. NO.	Intensity Of Solar Radiation	Ambient Temperature	Speed Of Wind *(m/s)*	Temperature Of Sky *(k)*
01	1000	35.8	2.6	296

The simulated values of meteorological parameters were tailored to the simulation's purpose. For the model verification with experimental data, the parameters were fine-tuned to match the experimental conditions. When exploring practical issues, typical meteorological parameters for Jammu City in summer were used.

Meteorological parameters typically considered include :

1. Temperature: air temperature plays a crucial role in weather forecasting.
2. Humidity: air humidity impacts weather conditions and atmospheric pressure.
3. Wind :
   Speed: wind speed is crucial for predicting weather patterns and storms.
   Direction: wind direction is essential for tracking weather events and understanding local climatic conditions.
4. Precipitation: (rain, snow, or hail) affects weather forecasts and emergency preparedness.
5. Air Pressure or Barometric Pressure: influencing weather conditions and forecasting

International Journal of Recent Development in Engineering and Technology
Website: www.ijrdet.com (ISSN 2347-6435(Online) Volume 14, Issue 12, December 2025)

6. Solar Radiation: affects temperature and weather patterns
7. Water Vapor Mixing Ratio: determines cloud formation and precipitation potential

These parameters are important for accuracy in weather forecasting and recognizing local climatic conditions. By modifying them according to the simulation's purpose, more accurate and relevant results can be ensured.

Air Density and Solution Settings: To capture the temperature-dependent air density, the Boussinesq hypothesis was applied for simplifying the solution process. The thermal expansion coefficient of air was set to 0.0037/K. The SIMPLEC algorithm was used to calculate the incompressible flow field. Convergence was achieved when the residuals for the continuity, momentum, k, and ε equations fell below $10^{(-3),}$ and the residuals for the energy and radiation equations fell below $10^{(-6)}$.

Simulation Verification: The simulation was verified by the experimental data from June 19, during which solar radiation intensity and air temperature remained relatively stable (approximately 930 W/m² and 37.8°C, respectively) from 10:00 to 14:30. Under these steady-state conditions, the heat transfer through the roof was analyzed. The ordinary roof's outer surface temperature peaked at 53.0°C at 14:30, while the photo-thermal roof's temperature rise was delayed by 2 hours, reaching a steady-state value of 37.0°C at 16:30. The inner surface temperature delay was calculated to be 5.5 hours. Consequently, the inner surface temperatures of the ordinary and photo-thermal roofs reached steady-state values of 43.2°C at 20:00 and 36.8°C at 23:00, respectively.

The phase delay was determined using the following equation:

$$\varphi = \sum D \div \sqrt{2} \times 57.3 - \text{arctg}(1/(1 + S1\sqrt{2}\alpha 1)) + \text{arctg}(1/(1 + Sn\sqrt{2}))$$

Numerical Calculation Results: Under the defined test conditions (solar radiation intensity: 930 W/m², air temperature: 37.8°C, insulation layer thickness: 100 mm, and average water temperature in the collector: 50°C), the numerical model was run. Preasuming a saturation rate of 0 due to the superior waterproofing performance, the computed temperatures for the conventional roof were 54.3°C (outer surface) and 38.7°C (inner surface). For the photo-thermal roof, the temperatures were 30.7°C (outer surface) and 28.1°C (inner surface).

The simulated values were marginally lower than the experimental data values, probably due to the neglect of radiation heat transfer between the wall and roof in the simulation.

Comparison of Experimental and Simulated Values: The simulated data values for the conventional roof closely aligned with the experimental values, with a maximum relative error (RE) of 8.3%. The photo-thermal roof simulations exhibited slightly greater deviations, with a maximum RE of 11.3%. Nevertheless, the root-mean-squared error (RMSE) of 3.1 indicates a overall satisfactory agreement between the experimental and simulated values, implying that the model is reasonably accurate.

III. Results And Analysis

Experimental Outcomes And Insights: The thermal insulation performance of the roofs was evaluated during the hot season in 2024. Experimental data from seven consecutive sunny days (June 15 to 22, 2024) was analyzed. The first three days experienced more cloud cover, affecting solar radiation intensity. The relationships between the roofs' surface temperatures and solar radiation intensity and air temperature. The data exhibited periodic changes, with solar radiation intensity reaching its maximum between 10:00 and 14:30 and outdoor air temperature fluctuating between 31.1°C and 38.6°C. The roof temperatures followed a similar pattern, but with varying peak times and temperature fluctuations.

The ordinary roof's outer surface temperature peaked at approximately 53.3°C between 13:00 and 14:30, while the inner surface temperature peaked at around 42.3°C between 18:00 and 19:30. However, the photo-thermal roof's outer surface temperature peaked at around 36.5°C between 15:30 and 16:30, and the inner surface temperature peaked at around 36.0°C between 22:00 and 24:00.

June 19 was selected as a typical day for further analysis, with data covering a full cycle from 0:30 on June 19 to 12:30 on June 20. This day had minimal cloud cover and represented typical local summer climate conditions.

On a typical day, the outdoor temperature fluctuated between 31.7°C to 38.2°C, while solar radiation peaked at 930 W/m² between 11:00 and 14:30. Notably, the photo-thermal roof's surface temperatures were substantially lower than the ordinary roof with peak temperatures of 37.0°C (outer) and 36.8°C (inner) compared to 53.0°C (outer) and 43.3°C (inner) for the ordinary roof.

International Journal of Recent Development in Engineering and Technology
Website: www.ijrdet.com (ISSN 2347-6435(Online) Volume 14, Issue 12, December 2025)

This translates to a significant reduction of 30.2% in outer surface temperature and a 15.0% reduction in inner surface temperature for the photo-thermal roof. The photo-thermal roof's design enables it to harness solar energy, minimizing heat gain and subsequent transfer to the inner surface. In contrast, the normal roof absorbs direct solar radiation, leading to higher surface temperatures.

The conventional roof's outer surface temperature reached its peak at 14:30, while its inner surface temperature peaked at 19:50, resulting in a time lag of 5 hours and 20 minutes. Conversely, the photo-thermal roof's outer surface temperature peaked at 16:30, and its inner surface temperature peaked at 22:00 representing a 2-hour delay for the outer surface and a 4-hour shift for the inner surface compared to the conventional roof. The temperature amplitude analysis demonstrated that the photo-thermal roof exhibited significantly lower amplitudes, with reductions of 78.0% and 72.6% for the outer and inner surfaces, respectively. This shows enhanced thermal stability for the photo-thermal roof.

The temperature difference between the inner and outer surfaces of both roofs follows a similar trend of solar radiation intensity. The maximum heat accumulation occurs when solar radiation is strongest, resulting in maximum thermal storage in the roof. The photo-thermal roof's design effeciently minimizes temperature fluctuations and heat gain, resulting in improved thermal performance.

The maximum temperature difference in the inner and outer surfaces was significantly lower for the photo-thermal roof (1.5°C) in comparison to the ordinary roof (14.2°C), specifying that the photo-thermal roof's heat transfer was decreased to nearly one-ninth of the ordinary roof's. This reveals the photo-thermal roof's superiority in insulation properties.

Effect of Water Saturation: To look into effect of changes in water saturation of insulation performance of the photo-thermal roof, simulations were carried out at various water saturation levels (0, 10%, 20%, and 30%). The solar radiation intensity was set at 1000 W/m², air temperature at 35.8°C, and roof insulation thickness at 100 mm. The water flow was regulated to maintain a constant pipe wall temperature of 50°C.

Increase in the water saturation resulted in a corresponding rise in the roof's effective thermal conductivity thereby enhancing heat transfer.

When water saturation increased from 0 to 30%, the ordinary roof's heat flux per unit area surged by 50.4% (from 65.9 W/m² to 99.1 W/m²). In the same manner, the inner surface temperature rose by 15.7% (from 39.4°C to 45.6°C), and the air temperature 400 mm below the roof increased by 11.1% (from 33.1°C to 36.8°C). Due to the enhanced heat transfer outer surface temperature got decreased (from 55.1°C to 53.2°C) and there was a drop in the vertical temperature gradient (from 52.3°C/m to 25.3°C/m). These findings suggest that increased water saturation in the roof insulation material boosts heat transfer. As the water saturation rose, the inner surface temperature and indoor air temperature also rose, in spite a potential decline in the temperature difference between the inner and outer surfaces. This resulted in enhanced heat radiation from the inner surface to the room. Especially, when water saturation increased from 0 to 10%, the ordinary roof's inner surface temperature increased rapidly by 4°C, and heat flux per unit area jumped by 21.0 W/m². In contrast, the photo-thermal roof's inner surface temperature and heat flux remained steady, with increases of only 0.1°C and 0.6 W/m², respectively.

As water saturation continued rising, the photo-thermal roof's temperature pattern displayed a consistent trend to the ordinary roof's though with much smaller changes. When water saturation increased from 0 to 30%, the photo-thermal roof's inner surface temperature increased by only 0.2°C (from 28.4°C to 28.6°C), and heat flux per unit area increased by 0.9 W/m² (from 11.5 W/m² to 12.4 W/m²). When compared to the ordinary roof, these increases were 96.8% and 97.3% lower, respectively.

The photo-thermal roof provided a more uniform indoor air temperature distribution by minimizing temperature fluctuations in the non-working area. In a nutshell, the photo-thermal roof outperformed the ordinary roof with smaller heat transfer, lower roof temperature, and lower indoor non-air-conditioned area temperature. While increased water saturation improved heat transfer in both roofs, its detrimental impact was significantly less pronounced in photo-thermal buildings.

Effect of Insulation Thickness: To achieve optimal thermal insulation, roof materials with low thermal conductivity are generally used, and their thickness plays a vital role. In areas with harsh temperatures, 95 mm thick rock wool boards are commonly used as roof insulation.

International Journal of Recent Development in Engineering and Technology
Website: www.ijrdet.com (ISSN 2347-6435(Online) Volume 14, Issue 12, December 2025)

To explore the connections between temperature, heat flux, and insulation thickness for both photo-thermal and ordinary roofs, simulations were performed with a solar radiation intensity of 1000 W/m², air temperature of 35.8°C, and s increases inner surface temperature and heat flux, while decreasing outer surface temperaturezero water saturation. The water flow was regulated to keep a constant pipe wall temperature of 50°C.

Insulation Thickness And Performance: With 100 mm insulation, the photo-thermal roof's outer surface temperature was 43.2% lower (31.1°C vs 55.1°C), inner surface temperature was 27.9% lower (28.4°C), and heat flux was 82.5% lower (11.5 W/m² vs 65.9 W/m²) in comparison to the conventional roof. The photo-thermal roof without insulation maintained satisfactory thermal performance, with 38.0% lower inner surface temperature (28.6°C vs 50.2°C) and 89.4% lower heat flux (19.2 W/m² vs 181.1 W/m²).

Combined Effects of Insulation Thickness and Water Saturation: Increased water saturation improved heat transfer, decrearing outer surface temperature and increasing inner surface temperature. With 100 mm insulation and 30% water saturation, the photo-thermal roof's inner surface temperature was 41.5% lower (28.6°C vs 45.6°C) and heat flux was 87.5% lower (12.4 W/m² vs 99.1 W/m²) comparably to the conventional roof. Even with reduced insulation thickness (25 mm) and high water saturation, the photo-thermal roof's inner surface temperature remained stable, around 28.5°C, only 2.5°C greater than the working area temperature.

IV. KEY TAKEAWAYS

This paper investigates the thermal insulation performance of a photo-thermal roof compared to a conventional roof in a hot summer and cold winter climate. The results show that:

1. The photo-thermal roof beats the conventional roof with smaller heat transfer, lower roof temperature, and lower indoor non-working area temperature. The heat transfer per unit area of the photo-thermal roof is 82.5% lower than the normal roof under simulated circumstances.
2. Water saturation notably influences insulation conduct, with a greater effect on the ordinary roof. When water saturation increases from 0 to 30%, the ordinary roof's inner surface temperature jumps up by 6.2°C, while the photo-thermal roof's temperature get up only by 0.2°C.
3. The photo-thermal roof's insulation conduct is less effected by changes in insulation material thickness. Even without insulation, the photo-thermal roof maintains satisfactory thermal conduct, with an inner surface temperature of 28.6°C in contrast to 50.2°C for the normal roof. This indicates that the insulation thickness of the photo-thermal roof can be lowered or even abolished.

REFRENCES

[1] Harmim, A.; Boukar, M.; Amar, M.; Haida, A. Simulation and experimentation of an integrated collector storage solar water heater designed for integration into building facade. Energy 2018, 166, 59–71.

[2] Gautam, K.R.; Andresen, G.B. Performance comparison of building-integrated combined photovoltaic thermal solar collectors (BiPVT) with other building-integrated solar technologies. Solar Energy 2017, 155, 93–102.

[3] Luo, K.; Ji, J.; Xu, L.; Li, Z. Seasonal experimental study of a hybrid photovoltaic-water/air solar wall system. Applied Thermal Engineering 2019, 169, 114853.

[4] Rahmani, F.; Robinson, M.A.; Barzegaran, M.R. Cool roof coating impact on roof-mounted photovoltaic solar modules at Texas Green Power microgrid. International Journal of Electrical Power & Energy Systems 2021, 130, 106932.

[5] Christoph, M.; Christoph, C.; Tilmann, E.K. Progress in building-integrated solar thermal systems. Solar Energy 2017, 154, 158–186.

[6] Ahmed, S.; Li, Z.; Javed, M.S.; Ma, T. A review on the integration of radiative cooling and solar energy harvesting. Materials Today Energy 2021, 21, 100776.

[7] Yu, G.; Yang, H.; Yan, Z.; Ansah, M.K. A review of designs and performance of facade-based building integrated photovoltaic-thermal (BIPVT) systems. Applied Thermal Engineering 2021, 182, 116081.

[8] Shao, N.; Ma, L.; Zhang, J. Experimental study on electrical and thermal performance and heat transfer characteristic of PV/T roof in summer. Applied Thermal Engineering 2019, 162, 114276.

[9] Ponechal, R.; Bar ˇnák, P.; Durica, P. Comparison of Simulation and Measurement in a Short-Term Evaluation of the Thermal Comfort Parameters of an Office in a Low-Carbon Building. Buildings 2022, 12, 349.

[10] Sourek, M.B. Façade solar collectors. Solar Energy 2006, 80, 1443–1452.

[11] Buonomano, A.; Forzano, C.; Kalogirou, S.A.; Palombo, A. Building-façade integrated solar thermal collectors: Energy-economic performance and indoor comfort simulation model of a water-based prototype for heating, cooling, and DHW production. Renewable Energy 2018, 137, 20–36.

[12] Chang, H.; Hou, Y.; Lee, I.; Liu, T.; Acharya, T.D. Feasibility Study and Passive Design of Nearly Zero Energy Building on Rural Houses in Xi'an, China. Buildings 2022, 12, 341.

[13] Gao, Y.; Shi, D.; Levinson, R.; Guo, R.; Lin, C.; Ge, J. Thermal performance and energy savings of white and sedum-tray garden roof: A case study in a Chongqing office building. Energy and Buildings 2017, 156, 343–359.

[14] Tong, S.; Li, H.; Zingre, K.T.; Wan, M.P.; Chang, W.C.; Wong, S.K.; Toh, W.B.T.; Lee, I.Y.L. Thermal performance of concrete-based roofs in tropical climate. Energy and Buildings 2014, 76, 392–401.

[15] Barone, G.; Buonomano, A.; Forzano, C.; Giuzio, G.F.; Palombo, A. Passive and active performance assessment of building integrated hybrid solar photovoltaic/thermal collector prototypes: Energy, comfort, and economic analyses. Energy 2020, 209, 118435.

[16] Long, J.; Jiang, M.; Lu, J.; Du, A. Vertical temperature distribution characteristics and adjustment methods of a trombe wall. Building and Environment 2019, 165, 106386.

[17] Bowen, B.D. Heat transfer-A basic approach, by M. Necati Öuzisik, 1985, 780 pages, McGraw-Hill Book Company, (U.S.). Canadian Journal of Chemical Engineering 1988, 66, 1036–1037.

[18] Zhou, J. Study on Microstructure and Energy Saving Characteristics of Rock Wool Board Used for Building External Wall Insulation System. Master's Thesis, Chang'an University, Xi'an, China, 2018.

[19] GB50736-2012. Design Code for Heating Ventilation and Air Conditioning of Civil Buildings. China Architecture & Building Press: Beijing, China, 2012.

[20] Heat Transfer under Periodic Heat Action. China Architecture & Building Press: Beijing, China, 1964.

[21] Manohar, K., Ramlakhan, D., Kochhar, G., Haldar, S. Biodegradable fibrous thermal insulation. Journal of the Brazilian Society of Mechanical Sciences and Engineering 28(1), 45–47 (2006).

[22] Panyakaew, S., Fotios, S. New thermal insulation boards made from coconut husk and bagasse. Energy and Buildings 43(7), 1732–1739 (2011).

[23] Pinto, J., et al. Characterization of corn cob as a possible raw building material. Construction and Building Materials 34, 28–33 (2012).

[24] Paiva, A., Pereira, S., Sá, A., Cruz, D., Varum, H., Pinto, J. A contribution to the thermal insulation performance characterization of corn cob particleboards. Energy and Buildings 45, 274–279 (2012).

[25] Zhou, X., Zheng, F., Li, H., Lu, C. An environment-friendly thermal insulation material from cotton stalk fibers. Energy and Buildings 42(7), 1070–1074 (2010).

[26] Agoudjil, B., Benchabane, A., Boudenne, A., Ibos, L., Fois, M. Renewable materials to reduce building heat loss: characterization of date palm wood. Energy and Buildings 43(2), 491–497 (2011).

[27] Chikhi, M., Agoudjil, B., Boudenne, A., Gherabli, A. Experimental investigation of new biocomposite with low cost for thermal insulation. Energy and Buildings 66, 267–273 (2013).

[28] Khedari, J., Charoenvai, S., Hirunlabh, J. New insulating particleboards from durian peel and coconut coir. Building and Environment 38(3), 435–441 (2003).

[29] Manohar, K. Experimental investigation of building thermal insulation from agricultural by-products. British Journal of Applied Science & Technology 2(3), 227–239 (2012).

[30] Yarbrough, D.W., Wilkes, K.E., Oliver, P.A., Graves, R.S., Vohra, A. Apparent thermal conductivity data and related information for rice hulls and crushed pecan shells. Thermal Conductivity 27, 222–230 (2005).

[31] Tangjuank, S. Thermal insulation and physical properties of particleboards from pineapple leaves. International Journal of Physical Sciences 6(19), 4528–4532 (2011).

[32] Vandenbossche, V., Rigal, L., Saiah, R., Perrin, B. New agro-materials with thermal insulation properties. In: 18th International Sunflower Conference, Mar del Plata, Argentina, pp. 949–954 (2012).

[33] Goodhew, S., Griffiths, R. Sustainable earth walls to meet the building regulations. Energy and Buildings 37, 451–459 (2005).

[34] Pruteanu, M. Investigations Regarding the Thermal Conductivity of Straw. Gheorghe Asachi Technical University, Jassy, Department of Civil and Industrial Engineering (2010).

[35] Al-Homoud, M.S. Performance characteristics and practical applications of common building thermal insulation materials. Building and Environment 40(3), 353–366 (2005).

[36] Moss, K. Heat and Mass Transfer in Building Services Design. London; New York: Routledge (1998).

[37] Progelhof, R.C., Throne, J.L., Ruetsch, R.R. Methods for predicting the thermal conductivity of composite systems: a review. Polymer Engineering & Science 16, 615–625 (1976).

[38] Sterner, E. Life-cycle costing and its use in the Swedish building sector. Building Research & Information 28(5-6), 387-393 (2000).

[39] Schmidt, M., Crawford, R.H. A framework for the integrated optimisation of the life cycle greenhouse gas emissions and cost of buildings. Energy and Buildings 171, 155-167 (2018).

[40] Robati, M., McCarthy, T.J., Kokogiannakis, G. Integrated life cycle cost method for sustainable structural design by focusing on a benchmark office building in Australia. Energy and Buildings 166, 525-537 (2018).

[41] Dwaikat, L.N., Ali, K.N. Green buildings life cycle cost analysis and life cycle budget development: practical applications. Journal of Building Engineering 18, 303-311 (2018).

[42] Vijaykumar, K.C.K., Srinivasan, P.S.S., Dhandapani, S. A performance of hollow clay tile (HCT) laid reinforced cement concrete (RCC) roof for tropical summer climates. Energy and Buildings 39(8), 886-892 (2007).

[43] Parker, D.S., Barkaszi, S.F. Roof solar reflectance and cooling energy use: field research results from Florida. Energy and Buildings 25(2), 105-115 (1997).

[44] Romeo, C., Zinzi, M. Impact of a cool roof application on the energy and comfort performance in an existing non-residential building. A Sicilian case study. Energy and Buildings 67, 647-657 (2013).

[45] Dimoudi, A., Androutsopoulos, A., Lykoudis, S. Summer performance of a ventilated roof component. Energy and Buildings 38(6), 610-617 (2006).

[46] Alvarado, J.L., Terrell, W., Johnson, M.D. Passive cooling systems for cement-based roofs. Building and Environment 44(9), 1869-1875 (2009).

[47] Megri, A.C., Achard, G., Haghighat, F. Using plastic waste as thermal insulation for the slab-on-grade floor and basement of a building. Building and Environment 33(2), 97-104 (1998).

[48] Gavenas, E., Rosendahl, K.E., Skjerpen, T. CO2-Emissions from Norwegian Oil and Gas Extraction. Norwegian University of Life Sciences, School of Economics and Business, 07-2015 (2015).

[49] Grossmann, K. Energetic Retrofit: Considering Socio-spatial Structures of Cities. Gaia - Ecological Perspectives for Science and Society (2014).

[50] Wolf, A., Schubert, J., Gill, B. Risiko energetische Sanierung? In: Großmann, K., Schafrin, A., Smigiel, C. (eds.) Energie und soziale Ungleichheit: Zur gesellschaftlichen Dimension der Energiewende in Deutschland und Europa, pp. 611-634. Springer Fachmedien Wiesbaden, Wiesbaden (2017).

[51] Michelsen, C., Müller-Michelsen, S. Energieeffizienz im Altbau: Werden die Sanierungspotenziale überschätzt? Ergebnisse auf Grundlage des ista-IWH-Energieeffizienzindex. Wirtschaft im Wandel 16(9), 447-455 (2010)

.